JOURNAL OF SPACECRAFT AND ROCKETS
Vol. 45, No. 5, September–October 2008

Sensitivity Analysis for the Dynamic Aeroelasticity of a Launch Vehicle

Franco Mastroddi,* Fulvio Stella,† Gian Mario Polli,‡ and Marilena Giangi§
University of Rome "La Sapienza," 00184 Rome, Italy

DOI: 10.2514/1.30725

A linearized aeroelastic analysis for a launch vehicle in the neighborhood of its transonic flight phase together with a local sensitivity study are presented. This investigation includes only dynamic aeroelastic instabilities, namely, flutter instabilities. Indeed, the launch vehicle considered for the applications is assumed to be initially free from other static instabilities like aeroelastic divergence, buckling, or from follower propulsive-force destabilizing effects, the study of which has not been included in the present paper. A modal description for the structural dynamics of the launcher in terms of the first nonzero natural frequencies and modes of vibration is carried out. Moreover, a reduced-order model for the unsteady transonic aerodynamics is obtained, performing several prescribed modal transient boundary conditions by laminar-based computational fluid dynamics. Thus, a modal input/output system identification for the aerodynamics, performed in the frequency domain, allows one to identify the linearized unsteady aerodynamic operator in the neighborhood of the specific transonic flight condition. Both the structural and aerodynamic models are finally employed in the aeroelastic coupled model given by the generalized Lagrangian equations of motion. An eigenanalysis, in terms of aeroelastic-system poles and complex eigenvectors on the linearized model, is performed to check the local dynamic stability of the launch vehicle. Finally, the proposed approach also allows one to give an evaluation of the uncertainty in the obtained stability scenario in terms of perturbing flight parameters like angle of attack, Mach number, flight speed, and air density.

I. Introduction

THE linearized aeroelastic stability for launch vehicles is a research field not as developed as that of the fixed wings, which has deeply characterized the history of the aviation and has a research development of about 100 years [1]. Nonetheless, in the authors' opinion, there are several topics in the aeroelasticity of rockets that deserve to be analyzed. An overview on the most relevant ones will be presented in the following to better clarify the contribution of the present paper in the framework of related activities.

A first set of issues can be collected under the general heading of global effects on a launch vehicle (LV) due to the application of the static propelling thrust force at its end edge. This topic is described by a multiphysics propulsion/structures/aerodynamics interaction. However, four different items on this issue are detailed in the following.

If one initially avoids the aerodynamic forces, structural instabilities may occur during the accelerating flight phase, induced by the interaction between the steady thrust load, elastic and inertial forces. This kind of instability is of static type, in that the linearized accelerated motion may present, dependent on the thrust magnitude, further multiple zero poles with corresponding nonrigid mode shape (namely, a critical mode shape) besides the zero poles associated with the rigid-body motion. There are many theoretical and numerical studies on these classical structural instabilities for rockets, and [2] is a pioneering analytic work on this issue, although it refers to a simplified homogeneous beam model. The study on the possible occurrence of this bucklinglike instability due to the accelerated motion is, of course, mandatory in the LV design phase.

Another effect induced by the axial static thrust force, which has immediate consequences on the LV structural dynamics, is a generalized softening of the nonzero eigenfrequencies, namely, a reduction of the in vacuo natural frequencies. Indeed, this effect is also joined with a very weak effect on the variation of the associated mode shapes.¶

A third well-known effect related to the application of the static thrust load/structures interaction is the so-called follower-force effect [2]. In addition, to further enrich the scenario of the eigensolutions or mode shapes related to multiple zero eigenvalues, this effect can also modify the nonzero frequency system response also in the nonvacuum (aeroelastic) case. Indeed, as showed in [3] for the case of the bending-torsion flutter analysis of a wing with a follower thrust force, this contribution may significantly affect the flutter stability margins and, therefore, it may change the frequency or the imaginary part of nonzero poles. This is not properly a static affect, although it is due to a static (follower) load. (This dynamic aeroelastic effect should be studied for an LV coherently, including in the analysis also the thrust vehicle control systems dynamics.)

When the static aerodynamic forces are also included in the LV model, the aeroelastostatic response and the possible occurrence of aeroelastic divergence instability can be evaluated. These represent a fourth example of global effects on the rocket system. Concerning this item, the research on fluid-structure interaction for an LV is at a considerable level of development [4]. Indeed, the level of integration of a computational fluid dynamics (CFD) code with the structural model allows also the evaluation of the aeroelastic flight-mechanics control derivatives [4,5].

Once a preliminary study on the global effects of the static thrust force has been performed, ensuring that no one of the aforementioned destabilizing effects are present, then a second typology of global

Received 28 February 2007; revision received 27 February 2008; accepted for publication 15 April 2008.

*Professor, Department of Aerospace Engineering and Astronautics, Via Eudossiana, 18.

†Professor, Department of Mechanics and Aeronautics, Via Eudossiana, 18.

‡Postdoctoral Fellow, Department of Aerospace Engineering and Astronautics, Via Eudossiana, 18.

§Postdoctoral Fellow, Department of Mechanics and Aeronautics, Via Eudossiana, 18.

¶This occurrence can be simply shown, in the very limited case of a simply supported homogeneous beam with an end-edge axial non-follower load N. The describing partial differential equation $EI\partial^4 w/\partial x^4 + N\partial^2 w/\partial x^2 + \mu\partial^2 w/\partial t^2 = 0$, gives zero variation for the modes of vibration; indeed, the mode shapes are $\phi_n(x) = A\sin(n\pi x/\ell)$ both for $N = 0$ and $N \neq 0$, but the natural frequencies are $\omega_n^2 = [EI(n\pi/\ell)^4 - N(n\pi/\ell)^2]/\mu$, and thus they are apparently subjected to a softening effect.

analysis can be performed. It consists of a dynamic stability study around the determined steady (actually, accelerated) solution for the global motion of the LV. The relevance of suitably describing the dynamic fluid/structure interaction for an LV, within this second stage of dynamic stability analysis, is highly emphasized in the current LV technical literature [6].

In the present paper, a linearized analysis for the dynamic instability of an LV during its transonic flight phase, as presented in [7], is proposed in a framework of analyses and studies that have been clarified previously. Specifically, it has been assumed that the LV system is free from static instability as from previously performed by first-stage analyses: indeed, the rigid accelerating body motion effects are not retained in the dynamic analysis, but the reference steady aerodynamic solution has been evaluated and then perturbed in the successive aerodynamic system identification procedure to study the linearized dynamic stability. Similarly, the softening effects on the structural dynamics due to the inertial forces have not been included in this dynamic analysis because the effects on the mode shape variations have been assumed negligible; conversely, the effects on the natural frequencies have been studied separately in a final sensitivity analysis. Finally, the LV-mass variation due to the combustion process of the propellant has been neglected in the time window in which evolution of the unsteady phenomenon is represented. This means, in practice, that it is assumed that the obtained linearized dynamic aeroelastic system representing the LV behavior has mechanical parameters constant in time.

The linearized mode-based approach for the dynamic aeroelastic analysis of an LV in [7] is used here. This approach was proposed on the basis of the specific development of some issues of fixed-wing aeroelasticity. Indeed, the mature development of the dynamic aeroelastic analysis of the fixed wing is due essentially to the capability of modeling 1) aerodynamics by means of linear unsteady flow conditions (linear potential flows [8]) and 2) structures by means of linear modal vibrations. (The use of model coordinates, instead of, for example, the physical ones in the space discretization, is particularly recommended if one studies global behaviors such as dynamic aeroelastic stability. Moreover, the reduced number of modal coordinates with respect to the physical ones keeps a good global level of accuracy and it also minimizes the aerodynamic computational efforts.) These model hypotheses are widely accepted and satisfied for most of the flight conditions of both civil and military aircraft. Therefore, several methods have been developed for linear aeroelastic stability and response analysis [1,9,10]. These procedures in time and frequency domains are currently available in many commercial codes typically used for aircraft aeroelasticity.

Whenever the flow conditions and/or the vibratory amplitude of the structures violate the hypotheses assumed for the models (transonic flows, viscosity effects, stall, large deformation for structures, etc.) two different procedures can be typically carried out:

1) A direct numerical simulation of the phenomenon (this concerns the field of computational aeroelasticity [9]) based, for example, on the use of a CFD Navier–Stokes solver for the flow, on a finite element nonlinear solver for the dynamics of the structure, and on a suitable boundary-condition interface performing the fluid-structure interactions [11,12] can be used. This approach is very difficult to be parametrically controlled in terms of given initial conditions. Furthermore, many simulations have to be performed to explore all the parametric conditions of the aeroelastic systems that are to be studied.

2) A linearization of the flow-structure behavior around the reference condition can be carried out. This linearization might be performed in two different ways: a) by means of a linearization of the original partial differential equation (PDE) mathematical model (e.g., a transonic small disturbance model for the aerodynamics) and then by performing a space-time discretization, or b) by means of a direct linearization of the aerodynamic numerical model by using CFD codes to produce the data necessary to perform such a linearization [7,13]. The disadvantage of this approach is due to its local nature. However, the apparent advantage is that in the local domain around the steady solution, the stability is ensured and parametrically controlled in a continuous set of possible initial conditions.

The lack of validated commercial codes and experimental tests on full-scale or scaled models for LV dynamic aeroelasticity [4,6,14–19] would address the present analysis toward a direct employment of direct numerical simulations. Nevertheless, this is typically very expensive from a computational point of view and not practically useful in an LV design phase. Thus, in [7] and in the present paper, the second approach (denoted as 2b), which uses a linearized unsteady aeroelastic analysis for an LV, was performed.

The structural dynamic model has been developed using a linear modal representation for the LV structures in terms of the lowest nonzero natural frequencies and corresponding natural mode shapes of vibrations. The modal selection employed in the analysis was based on a strain-energy criterion. Specifically, only the modes having finite elements on the fluid/structure interface with a strain-energy level greater than a fixed threshold have been included in the aeroelastic analysis. This structural model has been dynamically reduced in a Craig–Bampton [20] sense on the LV axis. Therefore, it consistently represents in the bandwidth of interest of the problem, the LV structural dynamics like the original 3-D finite element model does.

The linearized unsteady aerodynamic model has been obtained using the CFD data given by a laminar-Euler-based code and then postprocessed to obtain a global generalized representation for the aerodynamic unsteady loads, depending on the actual deformation state of the LV. This approach is within the framework of searching a reduced order model (ROM) for the unsteady aerodynamic operator, in the sense of reducing to the minimum the computational effort for a state-space representation of such an operator [21]. In the last decades, several contributions have been given on the development of ROMs for unsteady aerodynamics based on CFD data, both in frequency and in time domain, and all addressed the description of aeroelastic systems. For example, frequency domain ROMs were originally proposed in [22] by using indicial response, in [23] by using pulse transfer function, in [24] by using the panel method, by using the Volterra theory in [25–27], and the proper orthogonal decomposition (POD) in [28,29]. Moreover, in time domain, ROMs have been developed using the autoregressive moving average (ARMA) approach [30], the Volterra theory [31], the unit sample response [32], and the POD [33]. Within this wide-ROM scenario, the Volterra theory, POD, and ARMA approaches are able to identify both nonlinear and linear systems, whereas the other ROMs are able to represent only linear system dynamics around the steady-state solution. In the case in which the nonlinearities are given by the transonic flow conditions, as considered in the present paper, Dowell [9] indicates that, if the reference steady is accurately captured in terms of shock wave amplitude and location, the dynamic perturbation about the steady flow can by studied using a linearized model. This is the approach that has been followed in the present work to identify the dynamics of the unsteady aerodynamic operator around the steady transonic flow condition. More specifically, the linearized aerodynamic operator has been identified through an input/output time/frequency domain system identification approach on the basis of trial unsteady-boundary-condition inputs with shape given by the modal analysis of the LV structure. Specifically, the aeroelastic analysis of a 3-D geometry of an LV in the neighborhood of transonic flight conditions with prescribed angle of attack was carried out. The aerodynamic model considered for this linearization in the neighborhood of a given flow condition was able to take into account possible aerodynamic instabilities (e.g., the transonic buffet). On the other hand, other typical instabilities occurring in launcher aerodynamics due, for example, to flow separation (e.g., the stall buffet) will not be considered in this study. Thus, for example, some aerodynamic phenomena like separated or turbulent flows (see, for example, [19]) cannot be described by the proposed aerodynamic model. It is worth pointing out that the implemented modal unsteady aerodynamics used here for the dynamic stability is quite coupled. This issue is not typically taken into account in the classic dynamic aeroelastic analysis for LV [16,34] whenever contributions of all LV bending modes are independently taken into account. (However, the

approach in [16,34] had the important advantage of having allowed to tune the simplified aeroelastic model with the experimental data [18].)

Both the structural and aerodynamic models have been finally employed in the aeroelastic coupled model given by the generalized Lagrangian equations of motion. The specific LV considered for the application of the proposed approach is Vega LV. This is single-body multistage launcher developed by the European Space Agency with a liftoff weight of about 135 tons. Vega is a relatively small launcher (it has a medium diameter of 3 m and a length of about 30 m) for small satellite (with a maximum weight of 1500 kg and a low polar orbit of 700 km maximum) transport, and it is propelled by three solid-rocket motors for the first three stages and a liquid rocket motor for the last stage. The first launch has been scheduled by ESA for the end of the year 2008. To check the local stability of the Vega LV, an eigenanalysis (in terms of aeroelastic-system poles or eigenvalues) has been performed. (Incidentally, because of the frequency dependency of the identified aerodynamic operator, this eigen-analysis has been performed by means of an iterative procedure.) Finally, a sensitivity analysis of the obtained dynamic aeroelastic stability margins has been carried out with respect to several numerical and physical uncertainties, such as mesh discretization, number and type of mode shapes, angle of attack, Mach number, flight speed, and air density. This analysis has confirmed that the predictive capabilities of the adopted approach are effective and accurate for the dynamic aeroelastic analysis of an LV. In Sec. II, the physical and numerical aeroelastic model is presented (the reader is addressed to [7] for further details), whereas, in Sec. III, the numerical results of aeroelastic analysis and sensitivity are shown.

II. Theoretical Model for Linearized Aeroelasticity

The deformable body with respect to an equilibrium position is described by the displacement field $\mathbf{u}(\xi^\alpha, t)$, where $\xi^\alpha (\alpha = 1, 2, 3)$ are the material coordinates of the solid and t is the time coordinate. This vector field can be decomposed in a spectral way as

$$\mathbf{u}(\xi^\alpha, t) = \sum_{n=1}^{\infty} \boldsymbol{\Psi}^{(n)}(\xi^\alpha) q_n(t) \tag{1}$$

where the functions $\boldsymbol{\Psi}^{(n)}(\xi^\alpha)$ belong to a prescribed complete set of vector fields satisfying the homogeneous boundary conditions of the body, and the $q_n(t)$ are the associated generalized coordinates describing the body motion. If the summation is truncated to a finite number of terms equal to M, the body system will be referred to as space discretized. This hypothesis has been considered in the present model.

Assuming the previous relation for the description of the displacement field of the body and considering the principles of conservation for mass, momentum, and angular momentum, together with the constitutive assumption of elastic body (which is related to the elastic energy conservation principle), the following Lagrange equations of motion around the equilibrium position can be obtained:

$$\sum_{m}^{M} M_{nm} \ddot{q}_m + \frac{\partial \mathcal{E}}{\partial q_n} = e_n(q_n) \qquad n = 1, 2, \ldots, M \tag{2}$$

where M is the finite number of Lagrangian equations and generalized coordinates included in the analysis, and

$$M_{nm} := \iiint_V \rho(\xi^\alpha) \boldsymbol{\Psi}^{(n)}(\xi^\alpha) \cdot \boldsymbol{\Psi}^{(m)}(\xi^\alpha) \, \mathrm{d}V$$

are the coefficients of the (consistent) mass matrix, ρ is the solid mass density, $\mathcal{E}$ is the solid elastic energy, and

$$e_n = \oint_S \mathbf{t} \cdot \boldsymbol{\Psi}^{(n)}(\xi^\alpha) \, \mathrm{d}S \tag{3}$$

are the generalized forces obtained by projecting the body surface force field $\mathbf{t}$ (exerted by the flow on the body) on the function $\boldsymbol{\Psi}^{(n)}(\xi^\alpha)$. Neglecting the viscous terms in the expression of the aerodynamic forces, the surface pressure force field is given for a body in a flowfield by $\mathbf{t} = -(1/2)\rho_\infty V_\infty^2 C_p \mathbf{n}$, where ρ_∞ and V_∞ are the flow density and velocity at infinity, C_p is the aerodynamic pressure coefficient on the body surface, and $\mathbf{n}$ is the outward normal on the body surface. In this case, using the definition of dynamic pressure $q_D = (1/2)\rho_\infty V_\infty^2$, Eq. (3) becomes

$$e_n = -q_D \oint_S C_p(\xi^\alpha, t) \mathbf{n}(\xi^\alpha, t) \cdot \boldsymbol{\Psi}^{(n)}(\xi^\alpha) \, \mathrm{d}S \tag{4}$$

Note that these forces in the aeroelastic application typically depend on the motion, that is, on the Lagrange variables $q_n(t)$.

In the case of interest of linearized motion (e.g., this is the case of absence of geometric nonlinearities for the structure and linearized flow for aerodynamics) around the equilibrium position, Eq. (2) can be recast in the Laplace domain as

$$\sum_{m}^{M} s^2 M_{nm} \tilde{q}_m + \sum_{m}^{M} K_{nm} \tilde{q}_m = q_D \sum_{m}^{M} E_{nm}(s; M_\infty, V_\infty, \alpha) \tilde{q}_m \tag{5}$$

with $n = 1, 2, \ldots, M$, and where the tilde ($\tilde{}$) denotes Laplace transform with respect to time. K_{nm} is the stiffness matrix which models the linear portion of the structure elastic forces $(\partial \mathcal{E}/\partial q_n)$, M_∞ is the Mach number, and E_{nm} is the linearized unsteady aerodynamic operator [generalized aerodynamic force matrix (GAF)] typically dependent on the steady flow conditions M_∞, V_∞, and the angle of attack α. This parametric dependence can be exactly evaluated for linear space-discretized flows (e.g., linear potential flow [1,8,9]). However, it is also valid for the description of linearized flow conditions, such as those considered in the present analysis.

Assuming as shape functions $\boldsymbol{\Psi}^{(n)}(\xi^\alpha)$, the natural modes of vibrations of the structures, which are a complete set of functions on the body domain, the corresponding generalized coordinates represent the modal coordinates and K_{nm}, M_{nm} are the corresponding diagonal stiffness and modal-mass matrices. Moreover, the GAF matrix component E_{nm} relates in the Laplace domain the assumed mth modal motion on the body surface with the consequent projection of the aerodynamic pressure distribution on the nth shape function. It is worth emphasizing again that the magnitude of the number of such degrees of freedom is typically on the order of 10, fixing the accuracy as the same reached by the corresponding finite element (FE) discretization with an order thousands or millions of degrees of freedom. This is physically due to the higher velocity of convergence of the series in Eq. (1) for all times t whenever the shape functions $\boldsymbol{\Psi}^{(n)}$ are assumed to be the mode shape functions and not generic functions like, for example, the FE-shape functions. Indeed, this issue is namely true if the response problem under study has dynamics defined in the limited frequency bandwidth given by the assumed natural frequencies and, moreover, if the error used to define the accuracy is evaluated in a global way (e.g., taking the integral of the local error of the solution on the body domain). For this reason, in the dynamic aeroelastic applications (in particular, in the present paper), the modal description is widely employed as a space-discretization approach when global phenomena (like dynamic stability) are the main objective of the analysis. Moreover, the computational advantage for evaluating a GAF matrix on the order of 10, instead of evaluating one on the order of a thousand represents another relevant motivation for using the modal base in the present aeroelastic stability problem.

The procedure to identify the linearized unsteady aerodynamic model (GAF matrix) on the basis of the CFD data and the representation of the aeroelastic system in the state-space form is briefly presented in Secs. II.A and II.B, respectively. For details, the reader is referred to [7], where a validation of the procedure for a wing-airfoil test case is also reported.

A. Linearized Unsteady Aerodynamic Model (GAF Matrix)

The numerical procedure employed to identify the linearized unsteady aerodynamic operator in the neighborhood of a critical LV flight condition will be shown. Figure 1 gives an idea of the Vega LV geometry used in the following aerodynamic simulation together, with the aerodynamic mesh employed in the calculations (more detailed issues on LV geometry and mesh will be given in Sec. III). Note also that the influence of plume region on the aerodynamic unsteady loads has been considered in the present analysis.

The CFD simulation has been performed with the commercial code Fluent version 6.2.16 [35]. In particular, a dedicated module available in Fluent to upgrade mesh nodes positions at each time step of the simulations has been used. Three groups of mesh motion methods are available in Fluent to update the volume mesh in the deforming regions subject to the motion defined at the boundaries [35] 1) spring-based smoothing, 2) dynamic layering, and 3) local remeshing. In this paper, the spring-based smoothing method has been used.

When the motion of the body surface is assigned, it can be represented in modal coordinates using Eq. (1), and the consequent impermeability condition can be applied to the fluid boundary. In particular, if the motion is determined only by the generic mth mode, the corresponding body (LV) displacement field will be given by

$$\mathbf{u}_t(\xi^\alpha, t) = \boldsymbol{\Psi}^{(m)}(\xi^\alpha) q_m^t(t) \tag{6}$$

where the subscript and the superscript in $\mathbf{u}_t$ and $q_m^t(t)$ recall the trial nature of these functions employed in the identification of the aerodynamic operator, and, specifically, $q_m^t(t)$ is an arbitrary function of time which represents the time dependency of the motion given, in the space domain, by the mth modal shape. (This is equivalent to assigning the aerodynamic boundary conditions in terms of the following set of modal coordinates

$$(0 \quad 0 \quad \cdots \quad q_m^t(t) \quad 0 \quad \cdots \quad 0)$$

where only the mth component is not equal to zero.) In this case, differentiating Eq. (6), we have

$$d\mathbf{u}_t(\xi^\alpha, t) = \dot{q}_m^t(t) \boldsymbol{\Psi}^{(m)}(\xi^\alpha) dt \tag{7}$$

Therefore, the updated position of the grid node, with material coordinate ξ^α after the time dt, is given by

$$\mathbf{x}(\xi^\alpha, t + dt) = \mathbf{x}(\xi^\alpha, t) + \dot{q}_m^t(t) \boldsymbol{\Psi}^{(m)}(\xi^\alpha) dt \tag{8}$$

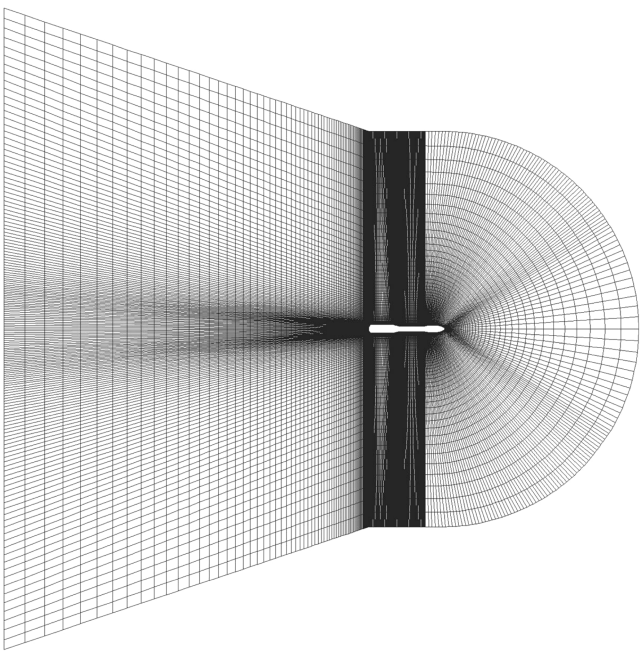

Fig. 1 Structured reference mesh used for CFD analysis.

This algorithm has been implemented through a user-defined function within the Fluent code. At each time step, the Fluent solver calls the routine, reads and computes the displacement fields for all moving nodes, and upgrades the mesh. More issues concerning the time-step definition will be addressed in Sec. II.B.

The pressure-coefficient field, due to the unsteady boundary condition defined in space by the generic mth mode, is indicated with $C_p^{(m)}(\xi^\alpha, t)$. This field generally contains a steady-state component given by the developed flow at the prescribed aerodynamic steady reference condition. This contribution has been filtered out by subtracting it from the global pressure field because the linearized description given by Eq. (5) includes perturbed quantities only. Thus, the corresponding generalized aerodynamic forces can be evaluated using Eq. (4), or

$$e_n^{(m)}(t) = -q_D \oint_S C_p^{(m)}(\xi^\alpha, t) \mathbf{n}^{(m)}(\xi^\alpha, t) \cdot \boldsymbol{\Psi}^{(n)}(\xi^\alpha) \, \mathrm{d}S \tag{9}$$

where $C_p^{(m)}(\xi^\alpha, t)$ is only the evaluated unsteady perturbed part of the pressure field due to the motion associated to the mth mode shape, whereas $\mathbf{n}^{(m)}(\xi^\alpha, t)$ in ξ^α and t is the unit normal associated with the mth mode shape considered as unsteady boundary motion (in the following, only the unsteady component of the pressure load will be indicated).

The surface integral performed on the surface S in Eq. (9) of the body has been numerically performed using a zeroth-order formula, considering every quantity constant in any aerodynamic panel composing the surface mesh and equal to the value at the centroid of the panel itself, that is,

$$e_n^{(m)}(t) \cong -q_D \sum_k^{N_c} C_p^{(m)}(\xi_k^\alpha, t) \mathbf{n}^{(m)}(\xi_k^\alpha, t) \cdot \boldsymbol{\Psi}^{(n)}(\xi_k^\alpha) A_k \tag{10}$$

where the subscript k represents quantities evaluated at the generic kth panel centroid and A_k is the surface area of the same panel.

As stated in Eqs. (2) and (5), the linearized unsteady aerodynamic operator in the Laplace domain, which transforms the modal coordinates $\tilde{q}_m$ into the generalized forces $\tilde{e}_n$, is described as

$$\tilde{e}_n = q_D \sum_m^M E_{nm}(s; M_\infty, V_\infty, \alpha) \tilde{q}_m \tag{11}$$

Thus, the simplest identification procedure for the GAF matrix operator E_{nm} is knowledge based on a given output $\tilde{e}_n$ due to a prescribed input $\tilde{q}_m$. Specifically, once a suitable input trial function $\tilde{q}_m^t$ is given for the mth mode, the corresponding displacement field on the body is given by Eq. (6). Therefore, assuming this motion for the aerodynamic mesh, the corresponding pressure-coefficient field is evaluated by the CFD code and, consequently, the nth generalized aerodynamic force computed by Eq. (10). After transforming this generalized force in the Laplace domain, the GAF matrix can be identified by

$$q_D E_{nm}(s; M_\infty, V_\infty, \alpha) = \frac{\tilde{e}_n^{(m)}}{\tilde{q}_m^t} \tag{12}$$

The choice of the trial input function $\tilde{q}_m^t$ is an important issue concerning both time/frequency crossing issues and CFD time/space discretization. Indeed, this function has to satisfy the compromise to be sufficiently impulsive in time (and, consequently, sufficiently wide in the frequency domain) to excite all the modes included in the aeroelastic analysis. At the same time, it cannot have a frequency band too large to induce numerical instability and lack of accuracy for the applied CFD solver. To this aim, the following Gaussian-like function

$$q_m^t(t) = C_m e^{-\{[t-(T/2)]/\kappa T\}^2} \tag{13}$$

has been used, where C_m is the impulsive function amplitude, T is the time window width, and κ (with $0 < \kappa < 1$) is a coefficient controlling the smoothness of the function at the boundary of its

domain. Indeed, the advantage given by this Gaussian function consists of the smoothness of such a function $q_m^t(t)$ at $t = 0$, which implies that it is here practically zero with its derivatives up to the second order. This is a relevant issue because the modal unsteady boundary conditions are given in terms of velocity, and therefore the smoothness of such a function is recommended [36].

The function parameters have been determined to have a correct (in terms of a space-aliasing problem) unsteady flow description up to a reduced frequency (Strouhal number) of $k = \omega\ell/V_\infty = 0.6$, and, finally, to have an amplitude C_m large enough to perturb the unsteady flow, but not so large as to induce numerical instability or nonlinear phenomena (indeed, a linearization of flow conditions is the objective of this approach). This function is depicted in Fig. 2 for $C_m = 0.325$. The time period T is related with the frequency band to be excited: specifically, as the interested frequency band is up to around 40 Hz, T has been chosen equal to 0.05 s, so that the corresponding Fourier transform signal has a constant frequency content up to about 70 Hz.

Finally, note that only Fourier transforms (not Laplace transforms) of signals with arbitrary shapes can be numerically performed. Therefore, substituting the Laplace transforms with the Fourier transform in Eq. (12) (namely, imposing $s = j\omega$), a frequency response function GAF matrix instead of a transfer function matrix is actually obtained.

B. Eigenanalysis of the Aeroelastic Model

Following the procedure illustrated in Sec. II.A, a linearized unsteady aerodynamic operator (GAF matrix) can be identified in the frequency domain. Nevertheless, considering Eq. (5), the stability analysis should be performed by solving the following eigenproblem for the eigenvalues s_n and the eigenvector $\mathbf{u}^{(n)}$

$$[s_n^2\mathbf{M} + \mathbf{K} - q_D\mathbf{E}(s_n; M_\infty, V_\infty, \alpha)]\mathbf{u}^{(n)} = 0 \tag{14}$$

where the GAF matrix should be known in all the complex planes (any values of s). Once the eigenvalues s_n and the eigenvectors $\mathbf{u}^{(n)}$ are determined, the free time response of the aeroelastic system can be written

$$\mathbf{q}(t) = \sum_n^M c_n\mathbf{u}^{(n)}e^{s_n t} + \text{CC terms} \tag{15}$$

where the obtained complex conjugated (CC) terms are not included in the summation. It is apparent (as in any standard linear analysis) that the nature of the eigenvalues s_n determines the system stability. However, the functional dependency of the aerodynamic operator $\mathbf{E}$ on the variable s is a relevant and characteristic issue of the aeroelastic problem for aircraft [9,10,13,37,38].

Indeed, this dependency is typically not of polynomial type, that is, the aerodynamic operator is not purely of differential type in time (e.g., for the linear potential aerodynamic of the fixed wing, this is of transcendental type [38]). Nevertheless, the GAF matrix $\mathbf{E}$ is only numerically known [see Eq. (12)] and only in the Fourier domain, or for the Laplace domain restriction $s = j\omega$. Therefore, two possibilities are available to solve the nonstandard eigenproblem given by Eq. (14):

1) An iterative procedure to capture the eigenvalues, assuming an analytic extension for the GAF matrix $\mathbf{E}$ from the imaginary axis on all the complex planes [1,38] may be used. The eigenvectors can be then evaluated by the corresponding homogeneous problem.

2) An analytical structure for the GAF matrix $\mathbf{E}$ as a function of the Laplace variable s may be assumed, and then determine it in a least-square sense minimizing the error of this evaluation with respect to the GAF data known in the Fourier domain by the CFD analysis.

The first methodology is the most common approach employed in the fixed-wing aeroelastic stability analysis, and a lot of iterative eigenmethods are implemented in commercial codes (e.g., k method, p method, g method) [1,10,38]. The second procedure has the advantage of transforming the nonstandard eigenproblem into a standard one and, as a by-product, describing the linearized aeroelastic system in a pure linear system of linear time ordinary differential equations. Only the first approach has been used in the present paper (actually a g method), although the second one has also been employed, giving practically the same aeroelastic stability scenario.

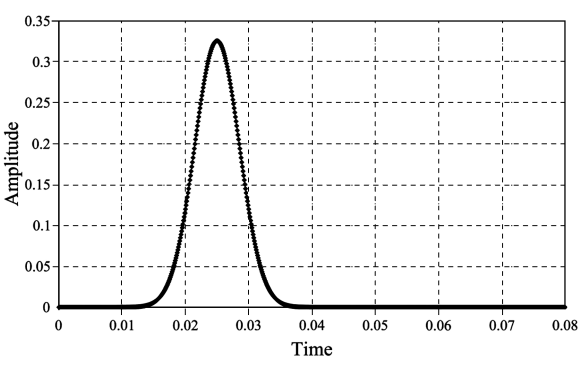

Fig. 2 Test function for CFD time input.

III. Numerical Simulations and Aeroelastic Sensitivities for a Launch Vehicle

A. Linearized Structural Model

The structural dynamics of the Vega LV have been studied using the MSC.NASTRAN commercial code. The structural dynamic analysis of the Vega LV has been provided by means of a detailed FE model based on a documented structural model of the LV. However, the FE model used for the aeroelastic analysis is based on a dynamic condensation of the detailed FE model, where every LV part is represented as a beam element characterized by a suitable axial and a flexural stiffness. Indeed, the modes are obtained after a dynamic condensation [20] process on the LV axis of the 3-D finite element model performed in the frequency bandwidth of interest. The results of the modal analysis on the beam model and the mode selection criterion for the aeroelastic analysis are presented in Sec. III.A.1. Section III.A.2 shows the extrapolation procedure used to evaluate the modal displacement directly on the aerodynamic mesh surface. This issue is quite relevant to impose the unsteady modal boundary conditions for the GAF matrix identification.

1. *Beam-Model Modal Analysis*

The modal analysis has been performed for a reference flight condition corresponding to a mass configuration, which is about 80% of the initial liftoff mass configuration (which is about 135,000 kg for this LV). This condition is reached approximately 20 s after the launch. The LV is considered in free–free boundary conditions to simulate the flight phase. Then, to select the modes for the LV aeroelastic analysis, two criteria have been considered: 1) axial modes are discarded, and 2) the nonaxial modes with a strain-energy level greater than 20% on the external part of the launcher are included in the aeroelastic analysis. The last criterion arises from the fact that an internal vibration condition, if uniformly distributed, is retained to be significant in the aeroelastic analysis. Therefore, four pairs of modes have been selected for the aeroelastic analysis, and Table 1 shows the first four natural nondimensional frequencies of the first four bending modes vibrating in two orthogonal transverse directions. Note that, to obtain nondimensional quantities, the actual

Table 1 Natural frequencies of the first four pairs of modes employed in the analysis (B = bending, PL = payload)

Modes	Nondimensional natural frequencies
1 B	1.00
2 B	2.42
2 B-PL	3.84
3 B	4.90

natural frequencies have been divided with respect to the first natural frequency. The same approach has also been applied in the presentation of the following aeroelastic results. Moreover, Figs. 3 and 4 show the mode shapes of the corresponding modes.

Specifically, the first two modes (Fig. 3a) have the same frequency due to the symmetry of the launcher, and they represent the first bending mode in two orthogonal transverse directions. The third and fourth modes (Fig. 3b) have, again, the same frequency for the same reason and represent the second bending mode in the two directions as well. The fifth and sixth modes (Fig. 4a) represent the second bending mode in the two orthogonal directions coupled with the motion of some internal equipment and payload. Finally, the seventh and eighth modes (Fig. 4b) represent the third free–free bending mode of the condensed model of the LV.

2. Expansion of the Mode Shapes on the Aerodynamic Mesh

Once the displacement field given by the modal shape has been obtained for the 1-D structural model, it is necessary to define the same field also for the 3-D aerodynamic mesh. Indeed, to complete the definition of the linearized aeroelastic model, it is necessary to (see also Sec. II.B) 1) impose every modal shape as an unsteady boundary condition to the CFD solver and 2) project the obtained pressure-coefficient field on the body surface for each mode shape function [see Eq. (4)].

For the first item, a dynamic-mesh dedicated package of the CFD solver has been used. Therefore, each mode shape obtained from the beam model (Figs. 3 and 4) has been expanded to the LV surface. The main hypothesis of the data extrapolation strategy is that any section orthogonal to the symmetry axis remains rigid during the motion (this is consistent with the beamlike behavior of the LV model). Furthermore, a linearized kinematics for the motion of the rigid sections has been assumed in the relationships relating the modal displacements and rotations of the beam-model nodes and the displacements on the LV surface points. An example of the first mode displacement field on the aerodynamic mesh of the 3-D Vega LV is depicted in Fig. 5. The extrapolation has been performed both on the centers of the aerodynamic surface panel elements for the force projection and on the nodes of the same aerodynamic surface panel for imposing the unsteady boundary conditions.

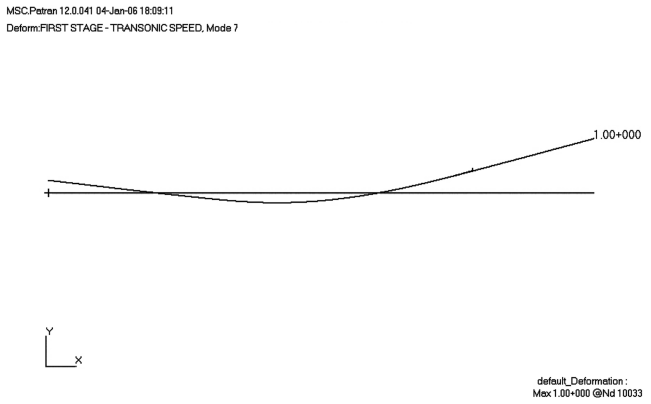

a) First mode

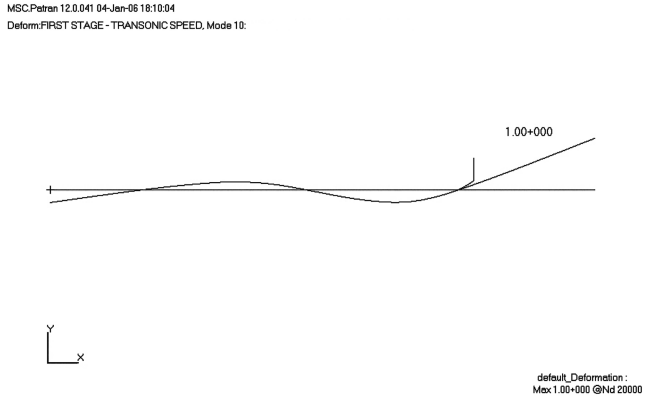

b) Second mode

Fig. 3 First and second free–free bending mode of the sticklike LV model.

B. CFD Mesh and Unsteady Aerodynamic Simulations

A structured mesh has been employed to study the steady and unsteady aerodynamics of the Vega LV. An important constraint to be satisfied using the structured mesh is the numerical stability of the solver during the mesh motion. The effect of small perturbations on the unsteady boundary conditions has been checked to ensure that the consequent deformation of the structured mesh does not significantly affect the mesh performance. The dimensions of the computational domain, in terms of size and spacing characteristics of the adopted mesh, have been subject to a systematic study. For example, the choice of a large domain, instead of a small or plumeless one (see Fig. 6), has been mainly motivated by the fact that the disturbance generated by the unsteady boundary conditions might be reflected by the computational-domain boundaries during the time simulation and then producing a fictitious pressure signal on the body surface.

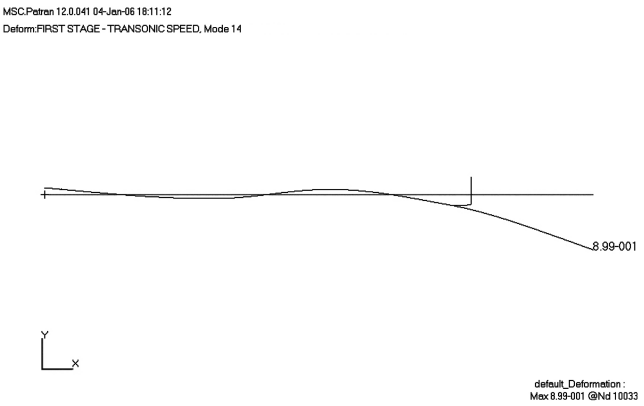

a) Third mode

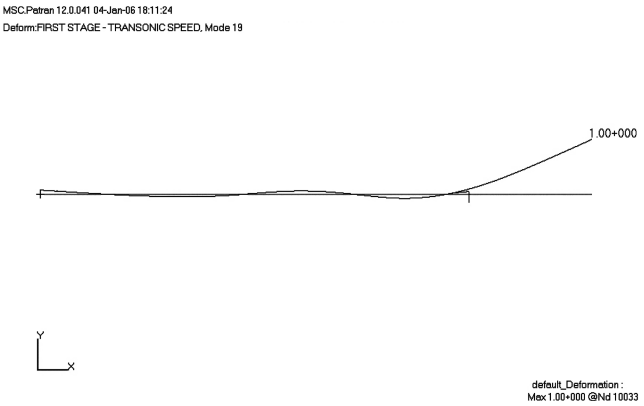

b) Fourth mode

Fig. 4 Third and fourth free–free bending mode of the sticklike LV model.

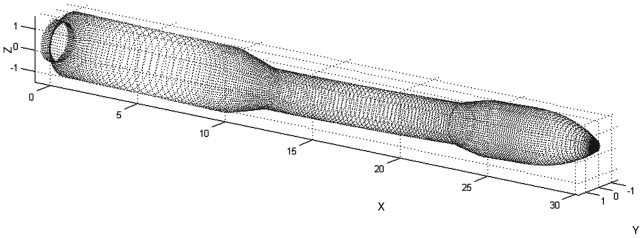

Fig. 5 Surface-expanded first mode shape of the LV 3-D model.

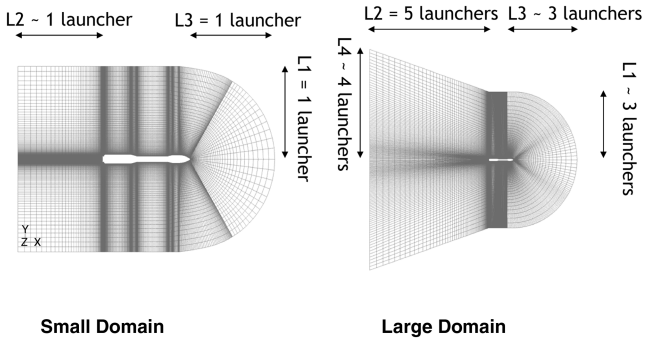

Fig. 6 Domain mesh options.

Indeed, the use of a small domain produces some spurious oscillations: this effect is presented in Fig. 7, in which the generalized aerodynamic force during the time simulation is reported. Therefore, in the present study, the large mesh was preferred to the small one (see Fig. 6).

Once the domain has been established, several mesh-sensitivity analyses are performed to define the reference mesh for the present study. Specifically, three different meshes have been considered: a coarse mesh with about 285,000 volume cells (mesh A), a nominal mesh with about 660,000 volume cells (mesh B), and a refined mesh with about 1.7×10^6 volume cells (mesh C). The results of this sensitivity on the pressure distribution on the LV surface have shown that mesh B (660,000 cells) practically reproduces the pressure distribution obtained by the finer mesh (mesh C). Thus, this mesh has been chosen as the reference mesh for the aeroelastic simulations. For the sake of conciseness, the results of this numerical convergence study for the reference steady solution are not reported in this paper. Indeed, from the results presented in Fig. 8, obtained using the three meshes for evaluating the unsteady aerodynamic response associated with the first bending mode, it is apparent that quite negligible differences are present between meshes B and C. This is shown both in time (Fig. 8a) and frequency domain (Fig. 8b). Indeed, considering the frequency domain analysis in Fig. 8b, these differences are more evident, particularly between meshes A and B, whereas the curves corresponding to meshes B and C are practically overlapped. Therefore, mesh B has been adopted for solving the unsteady problem under study. It is also worth pointing out that the unsteady case associated with the first bending mode has been selected for the unsteady CFD sensitivity analysis because this is the body modal motion which mainly influences the pressure distribution over the LV, and therefore the differences between the three meshes are the most evident.

To avoid numerical instability during the unsteady motion of the fluid boundary, a very short time step has been considered in the analysis together with a significant number of maximum iterations for convergence reasons. Specifically, the following parameters have been chosen in the analysis: a time step $\mathrm{TS} = 10^{-4}$ s and a number of maximum iterations within each time step $N_{\mathrm{iter}} = 50$. Although at the

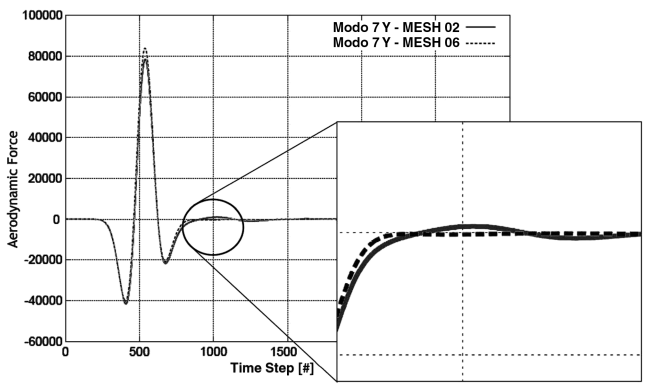

Fig. 7 Effects of pressure signal reflection on the first generalized aerodynamic force generated by the motion of the first bending mode.

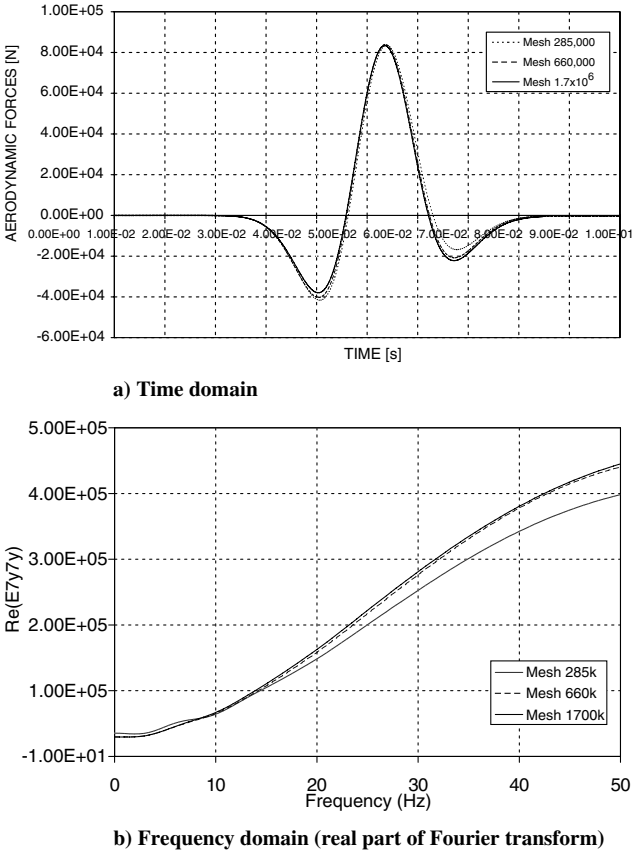

a) Time domain

b) Frequency domain (real part of Fourier transform)

Fig. 8 Mesh-sensitivity study on the first generalized unsteady aerodynamic force as due to the motion of the same first bending mode.

cost of greater CPU time, these choices avoided cell overlap and mesh distortions in every simulation performed, and guaranteed convergence of the CFD solver at every time step. The consequent direct CFD simulation with modal-shape-based motion in Fluent supplies the unsteady pressure coefficient.

The selected reference steady flow corresponds to a flight condition with Mach number $M_\infty = 0.855$, $V_\infty = 287.03$ m/s, and $\rho_\infty = 0.842$ kg/m^3. Also, the condition for the reference steady angle of attack has been fixed to $\alpha = 1$ deg. The corresponding reference aerodynamic field is then calculated using the laminar-based implicit steady solver available in Fluent code. Once the steady component has been filtered out from the unsteady solution, the resulting pressure disturbances have been projected on every assumed modal shape using a zeroth-order integral numerical scheme based on Eq. (10). The resulting generalized Lagrangian forces in the time domain have been calculated for all the assumed eight modes. However, the effect of motion associated with one mode on the generalized aerodynamic forces, obtained by projecting the induced unsteady pressure field on the corresponding orthogonal transverse mode, proved to be quite negligible. This indicated that the aerodynamic coupling potentially arising between transverse orthogonal modes in the presence of a reference steady angle of attack of 1 deg, is practically negligible. Indeed, Figs. 9a and 9b show the nondimensional aerodynamic forces achieved on the LV when the first in-plane and out-of-plane bending boundary motions are applied, respectively, in the unsteady moving mesh CFD procedure. In particular, in each figure, the integral projection on every mode shape considered in the aeroelastic analysis is reported, moreover, the first index in the legend represents the modal shape where the unsteady pressure fields are projected, whereas the second one denotes the number relative to the modal shape used for the boundary condition in the CFD simulation. Note that, in the following, the eight modes selected for the analysis have been denoted accordingly to the denomination provided by the FE code during their extraction; therefore, the first four modes in the xy plane are, respectively,

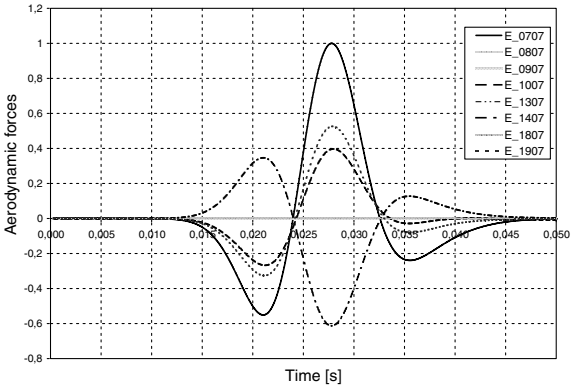

a) In-plane

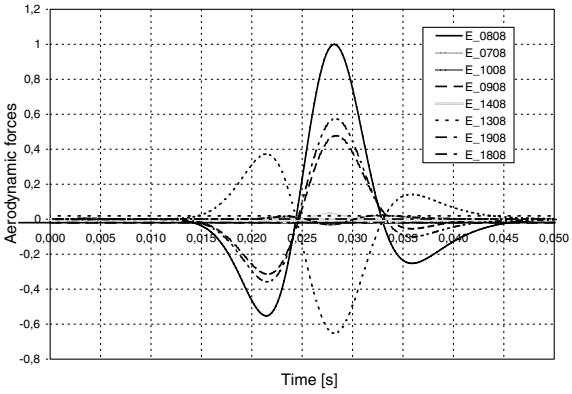

b) Out-of-plane

Fig. 9 Nondimensional aerodynamic forces due to the first in-plane and out-of-plane bending boundary motion.

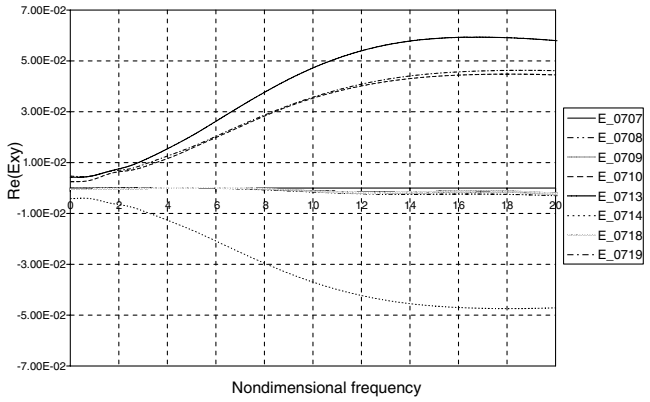

a) Real part

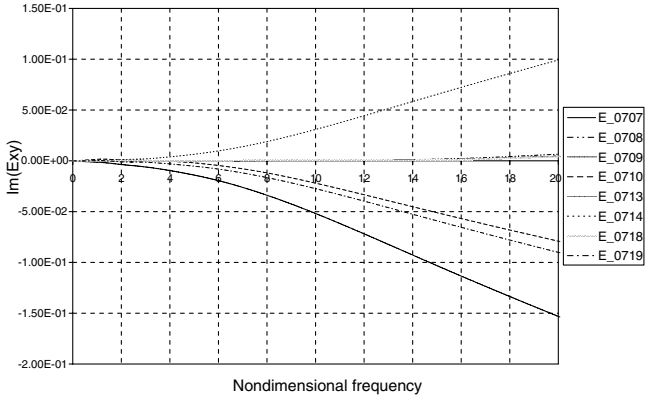

b) Imaginary part

Fig. 10 Nondimensional real and imaginary parts of the first row of the generalized aerodynamic forces matrix.

numbered as 07, 10, 13, and 19, whereas, those in the xz plane are 08, 09, 14, and 18. It is worth noting that, in Fig. 9a, the projections of the aerodynamic forces on the out-of-plane modes (respectively, the curves denoted as E_{0807}, E_{0907}, E_{1307}, E_{1807} in that figure) are negligible if compared with the in-plane projections (respectively, the curves denoted as E_{0707}, E_{1007}, E_{1407}, E_{1907} in that figure), in Fig. 9b, the out-of-plane projections (respectively, the curves denoted as $E_{0708}, E_{1008}, E_{1408}, E_{1908}$ in that figure) of the aerodynamic forces are small but not negligible with respect to the in-plane counterparts (respectively, the curves denoted as $E_{0808}, E_{0908}, E_{1308}$, E_{1808} in that figure). The reason of this different behavior is due to the nonzero angle of attack considered in the reference configuration of the LV. Indeed, the (small) incidence considered causes an unsymmetrization of the external aerodynamic flow over the LV. As the incidence angle lies in the xy plane, a motion of the surface boundary in that plane does not induce work on the modes lying in the xz plane (see Fig. 9a). On the contrary, when the surface boundary is moved in the xz plane, the resulting pressure field over the launcher can perform work on the modes lying in the xy plane (see Fig. 9b).

The generalized forces are transformed in the frequency domain with a fast Fourier transform (FFT) algorithm, and then the entries of the GAF matrix are evaluated using Eq. (12) in the Fourier domain, dividing these values by the FFT of the trial input function $q_m(t)$. Figures 10a and 10b show the real and the imaginary parts,

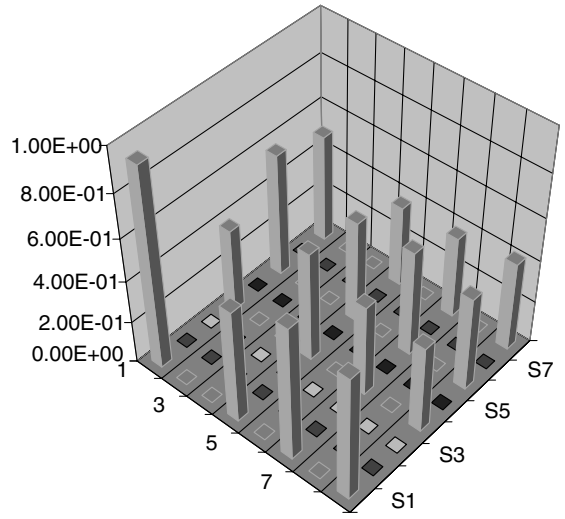

Fig. 11 Integrals of the moduli of the in-plane components of the GAF matrix.

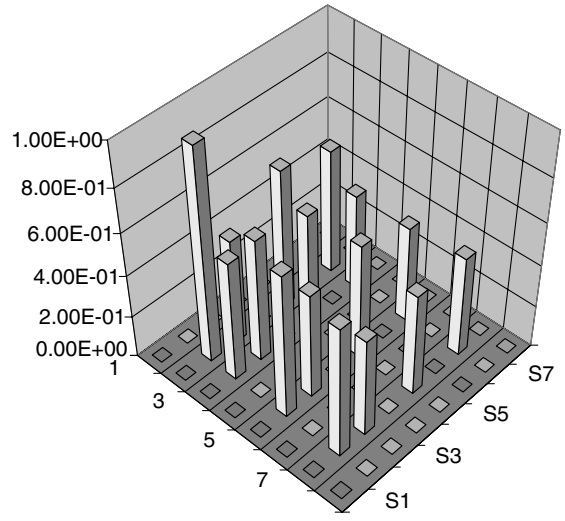

Fig. 12 Integrals of the moduli of the out-of-plane components of the GAF matrix.

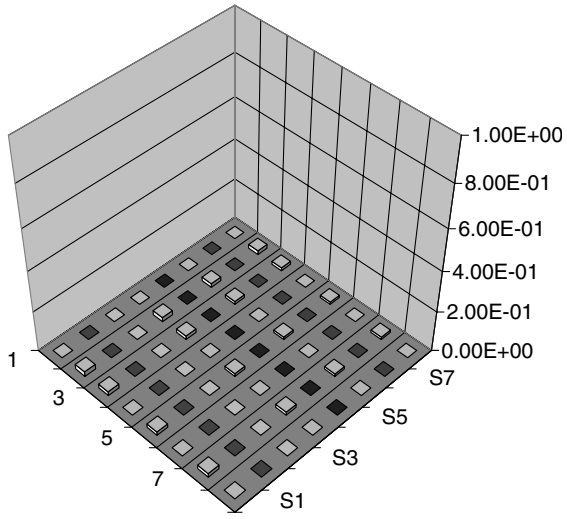

Fig. 13 Integrals of the moduli of the cross components of the GAF matrix.

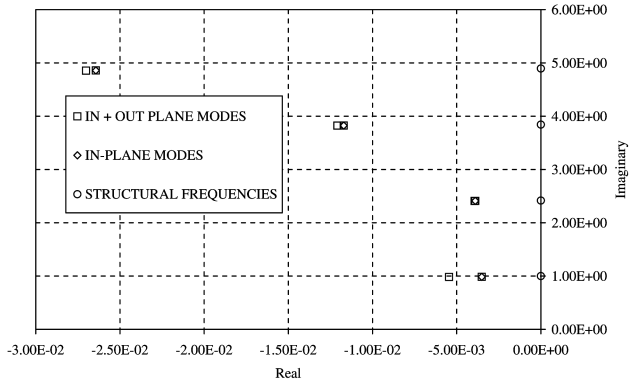

Fig. 14 Aeroelastic poles of the LV in the complex plane with and without out-of-plane modes.

respectively, of the first row of the synthesized GAF matrix. Again, one may note that the components of the GAF matrix associated with a pair of in-plane and out-of-plane modes are negligible with respect to the components of only in-plane or out-of-plane modes. This fact indicates that the aerodynamic coupling potentially arising between transverse orthogonal modes in presence of a reference steady angle of attack of 1 deg is weak. As a further confirmation of this analysis, in Figs. 11–13, the integrals of the modulus of the GAF matrix over the frequency band of interest are reported. Specifically, Fig. 11 shows the integral terms of the in-plane components, Fig. 12 shows the out-of-plane integral terms, and Fig. 13 the cross terms. It is apparent that only a negligible coupling is encountered between the in-plane and transverse modes. However, this result will be remarked upon in the next section when a discussion in terms of aeroelastic stability poles will be presented.

C. Aeroelastic Stability and Sensitivity Analysis

Once the structural and aerodynamic linearized models for the LV has been defined, the nonstandard eigenproblem associated with Eq. (14) could be performed for the considered flow conditions. Specifically, the considered flight parameters for the linearized aeroelastic analysis are those presented at the end of Sec. III.B, describing the reference flight condition. The obtained eigenvalues, having imaginary parts within a range compatible with the domain of satisfactory approximation for the GAF matrix (i.e., $0 < k < 1.1$, or $0 < \omega < 125$ rad/s) are depicted in Fig. 14 using a nondimensional representation (all the values have been divided by the first natural eigenfrequency).

As is apparent from Fig. 14, the aeroelastic system exhibits dynamic stability at this flow condition. Indeed, the original structural poles, which are marginally stable and composed of four pairs of coincident poles, tend to decouple each other and to become more stable, because of unsteady aerodynamic effects. This scenario is quantitatively described by the real part of the aeroelastic poles as presented earlier, which show that the so-called fairing aeroelastic modes (i.e., the third and fourth pair, see Figs. 4a and 4b) have a bit larger damping ratios (i.e., the ratio between the real and the imaginary part of the pole) than the others and that the second modes are less decoupled by the fluid/structure interaction. Before proceeding further, note that, in Fig. 14 also, the aeroelastic poles obtained considering only the in-plane modes are reported (in other words, poles obtained completely neglecting the coupling between in-plane and out-of-plane modal bending degrees of freedom). It is apparent that the poles associated with the in-plane modes are not practically affected by the presence of the out-of-plane modes. Moreover, one may observe that the poles associated with the in-plane modes are less aeroelastically stable than those associated with the out-of-plane modes. A quantitative analysis of the nature of the aeroelastic system can be done considering the associated aeroelastic eigenvector presented in Table 2, that is, the vectors $\mathbf{u}^{(n)}$ $(n = 1, 2, \ldots, 8)$ in Eq. (14). Indeed, the components of such eigenvectors indicate the structural modal contribution to each aeroelastic pole in the response [for all possible initial conditions, i.e., for all possible sets of coefficient c_n in Eq. (15)]. Thus, if one considers the (almost coincident) poles with lower damping ratio (whose aeroelastic eigenvectors are those depicted in columns 3 and 4 in Table 2), one may conclude that aeroelastic oscillation of the launcher in the considered flow condition would be mainly given by the combination of the second bending modes, respectively, in the wind plane and out of the wind plane.

Table 2 Table of aeroelastic eigenvectors associated with the reference aeroelastic system configuration

		Aeroelastic eigenvectors							
Modal components (magnitude)	1 out-of-plane	0.49	1.00	0.00	0.01	0.00	0.01	0.00	0.00
	1 in-plane	1.00	0.00	0.01	0.00	0.01	0.00	0.00	0.00
	2 in-plane	0.01	0.00	1.00	0.00	0.01	0.00	0.00	0.00
	2 out-of-plane	0.00	0.00	0.31	1.00	0.00	0.01	0.00	0.00
	3 in-plane	0.01	0.00	0.01	0.00	1.00	0.00	0.02	0.00
	3 out-of-plane	0.00	0.00	0.00	0.01	0.53	1.00	0.00	0.02
	4 in-plane	0.01	0.00	0.01	0.00	0.04	0.00	1.00	0.00
	4 out-of-plane	0.00	0.01	0.00	0.01	0.02	0.03	0.21	1.00
Modal components (phase-degrees)	1 out-of-plane	−42.1	0.0	−117.5	−176.9	−31.9	−19.7	86.1	160.1
	1 in-plane	0.0	98.1	−178.0	138.2	−21.3	−55.2	160.4	−61.2
	2 in-plane	−30.2	58.2	0.0	−35.2	−48.6	−86.6	151.1	−71.3
	2 out-of-plane	−52.1	−26.9	62.3	0.0	−66.2	−51.0	57.5	150.0
	3 in-plane	156.4	−118.3	165.0	122.9	0.0	−35.7	−22.8	115.8
	3 out-of-plane	127.3	161.7	−133.8	162.4	−15.4	0.0	−110.2	−22.0
	4 in-plane	−30.8	70.0	−28.0	−68.7	136.7	101.2	0.0	129.5
	4 out-of-plane	−62.3	−26.1	21.2	−30.9	122.4	137.0	−77.2	0.0

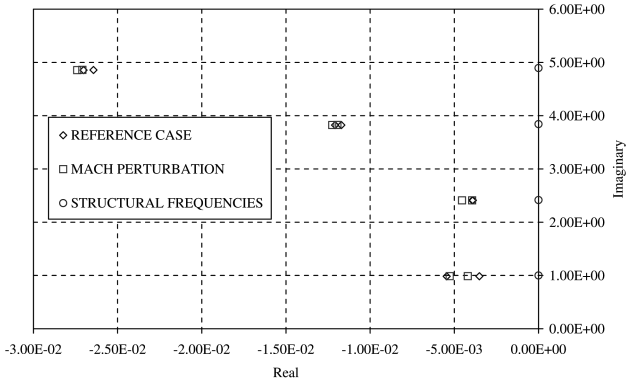

Fig. 15 Aeroelastic poles of the LV in the complex plane in the reference and Mach perturbed configurations.

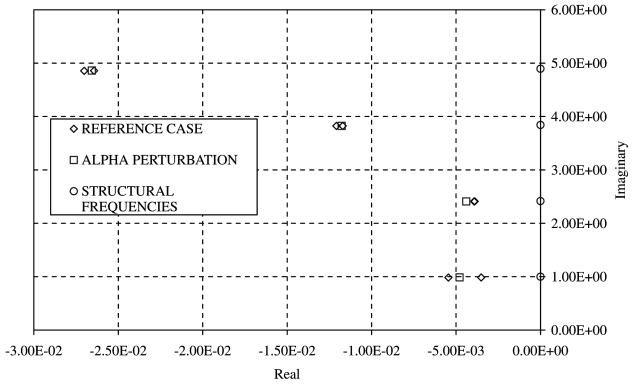

Fig. 16 Aeroelastic poles of the LV in the complex plane in the reference and zero incidence configurations.

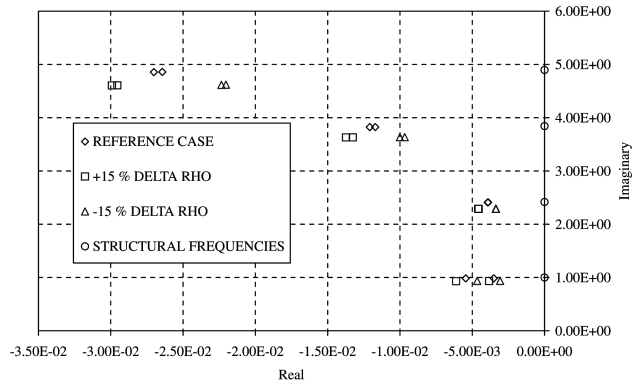

Fig. 17 Aeroelastic poles of the LV in the complex plane in the reference and perturbed flow condition by an air density variation of $\Delta\rho = \pm 15\%$.

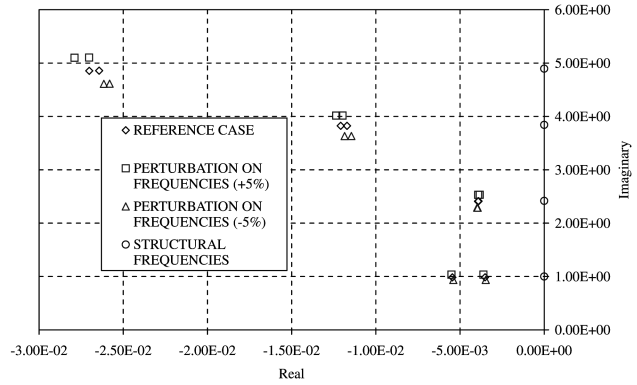

Fig. 18 Aeroelastic poles of the LV in the complex plane in the reference and perturbed structural eigenfrequencies by a $\Delta f_n = \pm 5\%$.

Starting from the previously discussed reference flow condition for the LV, several perturbations have been considered to study the sensitivity of the considered aeroelastic system. Specifically, a second set of simulations has been carried out using a different Mach number ($M_\infty = 0.875$, i.e., $\Delta M_\infty / M_{\infty,\mathrm{REF}} = 2.3\%$). The results of this analysis, in terms of aeroelastic poles in the complex plane, are shown in Fig. 15, in which the reference poles are also depicted for comparison. One may note that the local perturbation on the Mach number does not seem to perturb the aeroelastic stability margins so much. Moreover, one may observe that, except for the first out-of-plane pole, this perturbation is benign from the point of view of aeroelastic stability. In this regard, the fact that the first out-of-plane pole lowers its stability margin is due to the displacement of the sonic region along the body.

A third set of simulations regarded a perturbation on the angle of attack. Indeed, the analysis has been repeated considering a 0 deg angle of attack. As one may observe, in this case the axis symmetry of the flowfield over the launcher surface is preserved, thus one may expect that in-plane and out-of-plane modes are completely decoupled and coincident from the point of view of the natural frequencies and damping ratios. Figure 16 shows the results of this third sensitivity analysis in terms of aeroelastic poles in the complex plane in comparison to the poles of the reference case. Similar to the previously considered perturbation, one may notice that this perturbation is benign from the point of view of aeroelastic stability and that the aeroelastic poles are not perturbed very much by the variation of the angle of attack.

Finally, two other sensitivity analyses are reported in Figs. 17 and 18. Figure 17 shows the positions of the aeroelastic poles whenever a perturbation of $\pm 15\%$ of the density flow condition is considered. The figure shows that an increase in density induces a general stabilizing effect. Finally, Fig. 18 presents the same kind of sensitivity but induced by a variation of $\pm 5\%$ of all the eight natural frequencies assumed in the aeroelastic analysis. This study is equivalent to considering a softening/hardening perturbation on the structure stiffness due to a thrust-force intensity variation. One may note that a stiffening in the structural model generally induces a stabilizing effect in the aeroelastic poles, except for the second pair of modes which are weakly destabilized by the natural frequency increasing; this is probably due to the more coupled nature of this kind of aeroelastic pole.

IV. Conclusions

In this paper, a linearized dynamic aeroelastic stability and sensitivity analysis for the Vega LV during its transonic flight phase using an innovative approach are presented. Because of the local nature of the approach, the parametric-sensitivity analysis has been performed by a recalculation of the stability scenario in terms of aeroelastic poles and eigenvectors. Specifically, the aeroelastic analysis has been carried out by coupling the structural and the aerodynamic models by means of the use of the modal basis. Indeed, the structural dynamic model has been based on a modal representation for the LV structure employing the first eight nonzero natural frequencies and modes of vibration obtained via an FE solver. A specific criterion for the mode selection has been used to exclude from the analysis the modes associated with the internal vibration of the equipment and internal parts of the launcher. The thrust effects in the aeroelastic stability have been neglected, in particular, the softening effect caused by the thrust-load action has not been considered in the preliminary modal analysis; nonetheless, this effect has been taken into account in the final sensitivity analysis perturbing the natural frequencies around the reference solution. A ROM for the unsteady aerodynamics has been obtained using a CFD Euler-based unsteady solver. The predicted unsteady aerodynamic data have been postprocessed to obtain a fully coupled representation for the aerodynamic loads associated with the actual deformation state of the LV in terms of its modal description. The Lagrange equations

describing the global aeroelastic behavior in terms of the eight chosen modal coordinates have been obtained clearly showing the modal coupling given by the aerodynamic operator. Then, an eigenanalysis has been performed by means of an iterative procedure to check the dynamic aeroelastic stability of the Vega LV in the neighborhood of the flight phase under investigation. Finally, a sensitivity analysis in the neighborhood of a given flight condition in terms of Mach number, angle of attack, number of assumed modes, natural frequencies, and atmospheric density has also been performed, showing how this approach may represent a significant tool for an effective perturbation analysis of the aeroelastic performances of an LV.

Acknowledgments

This paper has been supported by ESA grant C19459. The authors wish to thank Francesco Capri for his contribution and support on obtaining some of the results presented in the paper.

References

[1] Bisplinghoff, R. L., Ashley, H., and Halfman, R. L., *Aeroelasticity*, Addison-Wesley, Cambridge, MA, 1955, pp. 1–14, 527–626.

[2] Peters, D. A., and Wu, J. J., "Asymptotic Solutions to a Stability Problem," *Journal of Sound and Vibration*, Vol. 59, No. 4, 1978, pp. 591–610. doi:10.1016/S0022-460X(78)80137-0

[3] Hodges, D. H., Patil, M. J., and Chae, S., "Effect of Thrust on Bending-Torsion Flutter of Wings," *Journal of Aircraft*, Vol. 39, No. 2, April 2002, pp. 371–376.

[4] Karpel, M., Yaniv, S., and Livshits, D. S., "Integrated Solution for Computational Static Aeroelasticity of Rockets," *Journal of Spacecraft and Rockets*, Vol. 35, No. 5, 1998, pp. 612–618.

[5] Zeiler, T. A., McGhee, D., and Brunty, J. A., "Preliminary Static Aeroelastic Analysis of Reusable Launch Vehicle Stability and Control Derivatives," *Journal of Spacecraft and Rockets*, Vol. 36, No. 1, 1999, pp. 67–74.

[6] Ericsson, L. E., "Hammerhead Wake Effects on Elastic Vehicle Dynamics," *Journal of Spacecraft and Rockets*, Vol. 34, No. 2, 1997, pp. 145–151.

[7] Capri, F., Mastroddi, F., and Pizzicaroli, A., "Linearized Aeroelastic Analysis for a Launch Vehicle in Transonic Flow," *Journal of Spacecraft and Rockets*, Vol. 43, No. 1, Jan.–Feb. 2006, pp. 92–104. doi:10.2514/1.13867

[8] Morino, L., "General Theory of Unsteady Compressible Potential Aerodynamics," NASA CR-2464, 1974.

[9] Dowell, E. H., *Modern Course in Aeroelasticity*, Kluwer, Dordrecht, The Netherlands, 1995.

[10] Hassig, H. J., "Approximate True Damping Solution of the Flutter Equation by Determinant Iteration," *Journal of Aircraft*, Vol. 8, No. 11, 1971, pp. 885–889.

[11] Tsai, H. M., Wong, A. S. F., Lai, J., Zhu, Y., and Liu, F., "Unsteady Flow Calculations with a Parallel Multiblock Moving Mesh Algorithm," *AIAA Journal*, Vol. 39, No. 6, 2001, pp. 1021–1029.

[12] Thomas, J. P., Dowell, E. H., and Hall, K. C., "Nonlinear Inviscid Aerodynamics Effects on Transonic Divergence, Flutter and Limit-Cycle Oscillations," *AIAA Journal*, Vol. 40, No. 4, 2002, pp. 638–646.

[13] Silva, W. A., Hong, M. S., Bartel, L. E., Piatak, D. J., and Scott, R. C., "Identification of Computational and Experimental Reduced-Order Models," *Proceedings of International Forum on Aeroelasticity and Structural Dynamics*, Netherlands Assoc. of Aeronautical Engineers Paper No. 2003-US-39, 2003.

[14] Ragab, M. M., "Buffet Loads Prediction for a Launch Vehicle and Comparison to Flight Data," *Journal of Spacecraft and Rockets*, Vol. 29, No. 6, 1992, pp. 849–855.

[15] Reding, P. J., and Ericsson, L. E., "Hammerhead and Nose-Cylinder-Flare Aeroelastic Stability Revisited," *Journal of Spacecraft and Rockets*, Vol. 32, No. 1, 1995, pp. 55–59.

[16] Dotson, K. W., Baker, R. L., and Sako, B. H., "Launch Vehicle Self-Sustained Oscillation from Aeroelastic Coupling, Part 1: Theory," *Journal of Spacecraft and Rockets*, Vol. 35, No. 3, 1998, pp. 365–373.

[17] Dotson, K. W., Baker, R. L., and Bywater, R. J., "Launch Vehicle Self-Sustained Oscillation from Aeroelastic Coupling, Part 2: Analysis," *Journal of Spacecraft and Rockets*, Vol. 35, No. 3, 1998, pp. 374–379.

[18] Ericsson, L. E., and Pavish, D., "Aeroelastic Vehicle Dynamics of a Proposed Delta II 7920-10L Launch Vehicle," *Journal of Spacecraft and Rockets*, Vol. 37, No. 1, 2000, pp. 28–38.

[19] Ericsson, L. E., "Unsteady Flow Separation can Endanger the Structural Integrity of Aerospace Launch Vehicle," *Journal of Spacecraft and Rockets*, Vol. 38, No. 2, 2001, pp. 168–179.

[20] Craig, R. R., and Bampton, M. C. C., "Coupling of Substructures for Dynamic Analysis," *AIAA Journal*, Vol. 6, No. 7, 1968, pp. 1313–1319.

[21] Dowell, E. H., and Tang, D. M., *Dynamics of Very High Dimensional Systems*, World Scientific Publishing, Singapore, 2003.

[22] Ballhaus, W. F., and Gootjian, P. M., "Computation of Unsteady Transonic Flows by Indicial Methods," *AIAA Journal*, Vol. 16, No. 2, 1978, pp. 117–124.

[23] Lee-Rausch, E. M., and Batina, J. T., "Wing Flutter Boundary Prediction Using Unsteady Euler Aerodynamic Method," *Journal of Aircraft*, Vol. 32, No. 2, 1995, pp. 416–422.

[24] Chen, P. C., Gao, X. W., and Tang, L., "Overset Field Panel Method for Unsteady Transonic Aerodynamic Influence Coefficient Matrix Generation," *AIAA Journal*, Vol. 42, No. 9, 2004, pp. 1775–1786. doi:10.2514/1.4390

[25] Silva, W. A., "Discrete-Time Linear and Nonlinear Aerodynamic Impulse Responses for Efficient CFD Analysis," Ph.D. Thesis, Faculty of the Dept. of Applied Science, College of William and Mary, Williamsburg, VA, Oct. 1997.

[26] Marzocca, P., Librescu, L., and Silva, W. A., "Volterra Series Approach for Nonlinear Aerodynamic Response of 2-D Lifting Surfaces," *42nd AIAA/ASME/ASCE/AHS/ASC Structures, Structural Dynamics & Materials Conference*, Vol. 3, AIAA, 2001, pp. 2047–2057.

[27] Raveh, D., Levy, Y., and Karpel, M., "Efficient Aeroelastic Analysis Using Computational Unsteady Aerodynamics," *Journal of Aircraft*, Vol. 38, No. 3, 1995, pp. 547–556.

[28] Hall, K. C., Thomas, J. P., and Dowell, E. H., "Proper Orthogonal Decomposition Technique for Transonic Unsteady Aerodynamic Flows," *AIAA Journal*, Vol. 38, No. 10, 2000, pp. 1853–1862.

[29] Thomas, J. P., Dowell, E. H., and Hall, K. C., "Three-Dimensional Transonic Aeroelasticity Using Proper Orthogonal Decomposition Based Reduced Order Models," *Journal of Aircraft*, Vol. 40, No. 3, 2003, pp. 544–551.

[30] Cowan, T. J., Arena, A. S., and Gupta, K. K., "Accelerating Computational Fluid Dynamics Based Aeroelastic Prediction Using System Identification," *Journal of Aircraft*, Vol. 38, No. 1, 2001, pp. 81–87.

[31] Silva, W. A., and Bartels, R. E., "Development of Reduced-Order Models for Aeroelastic Analysis and Flutter Prediction Using the CFL3DV6.0 Code," *Journal of Fluids and Structures*, Vol. 19, No. 6, 2004, pp. 729–745. doi:10.1016/j.jfluidstructs.2004.03.004

[32] Gaitonde, A., and Jones, D. P., "Reduced Order State-Space Models from the Pulse Responses of a Linearized CFD Schemes," *International Journal for Numerical Methods in Fluids*, Vol. 42, No. 6, 2003, pp. 581–606. doi:10.1002/fld.527

[33] Beran, P. S., Lucia, D. J., and Pettit, C. L., "Reduced Order Modeling of Limit Cycle Oscillation for Aeroelastic Systems," *Journal of Fluids and Structures*, Vol. 19, No. 5, 2004, pp. 575–590. doi:10.1016/j.jfluidstructs.2004.04.002

[34] Ericsson, L. E., and Reding, J. P., "Fluid Dynamics of Unsteady Separated Flow, Part 1: Body of Revolution," *Progress in Aerospace Sciences*, Vol. 23, No. 1, 1986, pp. 1–84. doi:10.1016/0376-0421(86)90005-9

[35] Fluent 6.2 User's Guide, Fluent, Lebanon, NH, Jan. 2005.

[36] Lisandrin, P., Carpentieri, G., and Van Tooren, M., "Investigation over CFD-Based Models for the Identification of Nonlinear Unsteady Aerodynamics Responses," *AIAA Journal*, Vol. 44, No. 9, Sept. 2006, pp. 2043–2050. doi:10.2514/1.18726

[37] Morino, L., Mastroddi, F., De Troia, R., Ghiringhelli, G. L., and Mantegazza, P., "Matrix Fraction Approach for Finite-State Aerodynamic Modeling," *AIAA Journal*, Vol. 33, No. 4, 1995, pp. 703–711.

[38] Gennaretti, M., and Mastroddi, F., "Study of Reduced-Order Models for Gust-Response Analysis of Flexible Fixed Wing," *Journal of Aircraft*, Vol. 41, No. 2, March–April 2004, pp. 304–313. doi:10.2514/1.9325

G. Agnes
Associate Editor